

Revisiting the Bohr Model of the Atom through Brownian Motion of the Electron

Vasil Yordanov

v.yordanov@phys.uni-sofia.bg

Faculty of Physics, Sofia University,

5 James Bourchier blvd., 1164 Sofia, Bulgaria

February 25, 2025

Abstract

In this work, we refine the Bohr model of the hydrogen atom by describing the motion of the electron through a single real-valued stochastic process, effectively realizing Brownian motion under the Born rule. Our approach derives the electron's stochastic equation of motion from the Fokker–Planck equation while ensuring the particle always maintains a definite – albeit random – position. This feature obviates the need for wave function collapse as invoked in the Copenhagen interpretation. Instead, the wave function serves as a tool to compute the electron's drift velocity. Building on this, we develop modified stochastic equations in spherical coordinates, tailored to the spherical symmetry of the hydrogen atom. We show that these equations reproduce the correct average radial and angular kinetic energies, matching operator-based quantum mechanical predictions. Numerical simulations confirm the stability of electron trajectories and, as expected, recover the probability distribution prescribed by the Born rule. At very short timescales, however, single-electron probability distributions may deviate from wave function–based predictions due to insufficient ensemble averaging. Taken together, these findings offer an alternative perspective on atomic structure and highlight the potential of using wave function–derived drift velocities within a single stochastic process to capture quantum dynamics in the hydrogen atom.

1 Introduction

The hydrogen atom has been pivotal in shaping our understanding of atomic structure and quantum mechanics. Early atomic models, such as Thomson's “plum pudding” model [1] and Rutherford's nuclear model [2], established the concept of electrons within atoms but could not adequately explain atomic stability and spectral lines. Bohr's model [3] introduced quantized electron orbits to address these issues, successfully explaining the discrete spectral lines of hydrogen but relied on classical orbits with imposed quantum conditions.

While Schrödinger's wave mechanics [4] provided a probabilistic framework for electron behavior, questions remain about the underlying nature of quantum phenomena and the reconciliation of quantum probabilities with classical intuition [5].

In this work, we propose an approach we call Born–Fokker–Planck Stochastic Quantum Mechanics (Stochastic QM), a novel framework that describes the electron’s motion via a single real-valued stochastic process. Here, the Born rule is taken as the fundamental basis for the probability distribution of the electron’s position. By employing the Fokker–Planck equation, we derive a stochastic equation of motion that is consistent with this distribution, thereby providing a particle-trajectory picture without invoking wave function collapse.

When applied to the hydrogen atom, Born–Fokker–Planck Stochastic QM yields stochastic equations of motion that not only reproduce the average energies and probability distributions predicted by conventional quantum mechanics but also offer new insights into the electron’s trajectory. Our simulations reveal that for electronic states with complex radial or angular structures, extended simulation times (i.e., sufficient ensemble averaging) are required to achieve convergence to the theoretical distributions.

Because Born–Fokker–Planck Stochastic QM provides a framework in which the electron’s position is both well-defined and inherently stochastic, it offers a potential basis for future weak measurement experiments [6, 7, 8]. Such experiments could provide more precise tests of quantum mechanics and yield deeper insights into ultrafast electron dynamics, ultimately guiding the design of next-generation quantum measurement schemes.

2 Comparison with Nelson’s Stochastic Mechanics

Nelson’s Stochastic Mechanics [9, 10] is one of the most well-known attempts to reformulate quantum theory in terms of Brownian motion. In Nelson’s framework, the evolution of a quantum particle is described by two Wiener processes – one evolving forward in time and the other backward. Although both processes are constructed on the same statistical foundation (sharing the same diffusion constant and underlying probability structure), they differ in their time orientation. In the forward process, the stochastic increments are defined so as to be independent of past coordinate values, whereas in the backward process, the increments are independent of future coordinate values. Appropriate consistency conditions are imposed on these two time-asymmetric processes so that their combined description reproduces the predictions of the Schrödinger equation.

Several subsequent formulations [11, 12, 13, 14, 15] extend this idea by employing the Hamilton–Jacobi–Bellman equation. In these approaches, two perfectly correlated stochastic processes – one corresponding to the real part and the other to the imaginary part of the particle’s coordinates – are used to capture the full phase information of the wave function.

In contrast, our Born–Fokker–Planck Stochastic QM requires only a single real-valued stochastic process to describe the particle’s motion. In our approach, the wave function is used solely to compute the drift velocity via the gradient of the logarithm of its modulus; that is, only the amplitude is used in determining the particle’s stochastic dynamics, while the phase is ignored when formulating the stochastic equation of motion. However, the phase still plays an essential role when solving the Schrödinger equation to obtain the full wave function. Rather than deriving the Schrödinger equation from the interplay of forward and backward processes, we take the Schrödinger equation as given and use it to determine the drift velocity

according to the Born rule.

There has been prior attempts to apply Stochastic Mechanics to the hydrogen atom, but using two stochastic equations. In their work, Truman and Lewis [16] employed Stochastic Mechanics theory to analyze the ground state of the hydrogen atom, primarily focusing on the radial equation of motion and first hitting times. For the angular stochastic equations, they utilized the Stroock equation [17] to model Brownian motion on the sphere S^2 . However, they provided the stochastic equation of motion on the sphere without delving deeper into these equations. Their approach involved constraining the process in \mathbb{R}^3 to remain on the sphere by incorporating projection and drift terms. In the current work, we employ a single real-valued stochastic process and express Brownian motion directly in spherical coordinates, thereby capturing the motion intrinsically on S^2 according to the framework introduced by Itō [18]. Although we do not adopt Stroock's approach [17], we acknowledge the existence of a third method to describe Brownian motion on a sphere, introduced by Price and Williams [19]. For more details, refer to the work of Van Der Berg [20]. Notably, both Stroock's and Price and Williams' approaches use extrinsic coordinates embedded in \mathbb{R}^3 , unlike Itō's approach [18], which explicitly incorporates the manifold's geometry through the metric tensor and Christoffel symbols.

3 Derivation of the Stochastic Equation of Motion for a Quantum Particle from the Born Rule and the Fokker–Planck Equation

In this section, we develop a stochastic equation of motion for a quantum particle by drawing an analogy with Brownian motion. Our goal is to construct a single real-valued stochastic process capable of simulating the stationary states of systems such as the hydrogen atom; however, the derived equation is also valid for non-stationary cases.

Consider a particle with position $\mathbf{x} \in \mathbb{R}^3$. We postulate that its infinitesimal displacement obeys the stochastic differential equation:

$$dx^k = v^k dt + \sigma^k dW^k, \quad k = 1, 2, 3, \quad (3.1)$$

where v^k denotes the (as yet undetermined) drift velocity in the k -th coordinate, dW^k are increments of independent Wiener processes (standard Brownian motions), and dt is the time increment.

The probability density $P(\mathbf{x}, t)$ associated with this process satisfies the Fokker–Planck equation:

$$\partial_t P(\mathbf{x}, t) = -\nabla \cdot [\mathbf{v}(\mathbf{x}, t) P(\mathbf{x}, t)] + \frac{1}{2} \sum_k (\sigma^k)^2 \nabla^2 P(\mathbf{x}, t). \quad (3.2)$$

Here, we postulate that, for each coordinate, the square of the diffusion coefficient is given by $(\sigma^k)^2 = \frac{\hbar}{m}$, thereby relating it to the particle's mass and Planck's constant.

According to the Born rule, the probability density for a quantum particle's position is given by:

$$P(\mathbf{x}, t) = |\psi(\mathbf{x}, t)|^2, \quad (3.3)$$

where the wave function $\psi(\mathbf{x}, t)$ satisfies the Schrödinger equation:

$$i\partial_t \psi(\mathbf{x}, t) = -\frac{\hbar^2}{2m} \Delta \psi(\mathbf{x}, t) + V(\mathbf{x}, t) \psi(\mathbf{x}, t). \quad (3.4)$$

If we define a complex action function $J(\mathbf{x}, t) = J_R(\mathbf{x}, t) + i J_I(\mathbf{x}, t)$, the wave function can be expressed as:

$$\psi(\mathbf{x}, t) = e^{-\frac{1}{\hbar}(J_R(\mathbf{x}, t) + i J_I(\mathbf{x}, t))}, \quad (3.5)$$

Substituting this form into the Born rule yields:

$$P(\mathbf{x}, t) = |\psi(\mathbf{x}, t)|^2 = e^{-\frac{2}{\hbar} J_R(\mathbf{x}, t)}. \quad (3.6)$$

Thus, the real part of the action can be written as:

$$J_R(\mathbf{x}, t) = -\hbar \log |\psi(\mathbf{x}, t)|. \quad (3.7)$$

Substituting $P(\mathbf{x}, t)$ into the Fokker–Planck equation and performing the necessary algebra (i.e., differentiating $P(\mathbf{x}, t)$ with respect to time and space) leads to the relation:

$$-\partial_t J_R(\mathbf{x}, t) = \left(\mathbf{v}(\mathbf{x}, t) + \frac{1}{m} \nabla J_R(\mathbf{x}, t) \right) \cdot \nabla J_R(\mathbf{x}, t) - \frac{1}{2} \hbar \nabla \cdot \left(\mathbf{v}(\mathbf{x}, t) + \frac{1}{m} \nabla J_R(\mathbf{x}, t) \right) \quad (3.8)$$

This is a first-order linear partial differential equation for the unknown drift velocity $\mathbf{v}(\mathbf{x}, t)$, with time t treated as a parameter.

Defining the auxiliary vector field:

$$\mathbf{u}(\mathbf{x}, t) = \mathbf{v}(\mathbf{x}, t) + \frac{1}{m} \nabla J_R(\mathbf{x}, t), \quad (3.9)$$

the equation can be rewritten as:

$$\nabla \cdot \mathbf{u}(\mathbf{x}, t) - \frac{2}{\hbar} \mathbf{u}(\mathbf{x}, t) \cdot \nabla J_R(\mathbf{x}, t) = \frac{2}{\hbar} \partial_t J_R(\mathbf{x}, t). \quad (3.10)$$

In the stationary case – when the potential $V(\mathbf{x})$ is time-independent – the wave function can be expressed as:

$$\psi(\mathbf{x}, t) = \psi(\mathbf{x}) e^{i \frac{E}{\hbar} t}, \quad (3.11)$$

the probability density $P(\mathbf{x})$ becomes time-independent. Consequently, from Eq (3.6), $J_R(\mathbf{x})$ is also independent of time, and Eq. (3.10) reduces to:

$$\nabla \cdot \mathbf{u}(\mathbf{x}) - \frac{2}{\hbar} \mathbf{u}(\mathbf{x}) \cdot \nabla J_R(\mathbf{x}) = 0 \quad (3.12)$$

A general solution to this equation is:

$$\mathbf{u}(\mathbf{x}) = \mathbf{C}(t) e^{\frac{2}{\hbar} J_R(\mathbf{x})}, \quad (3.13)$$

where $\mathbf{C}(t)$ is an arbitrary (time-dependent) constant vector. In the stationary case, if we require that the additional contribution vanishes (i.e. choose $\mathbf{C}(t) = 0$), then $\mathbf{u}(\mathbf{x}) = 0$.

Recalling Eq. (3.9), we obtain:

$$\mathbf{v}(\mathbf{x}) = -\frac{1}{m} \nabla J_R(\mathbf{x}). \quad (3.14)$$

In contrast, in certain formulations of Stochastic Mechanics that employ complex velocities [11, 21, 22, 12, 14, 15], the drift velocity is expressed as: $\mathbf{v}(\mathbf{x}) = i \nabla J(\mathbf{x})$, where $J(\mathbf{x})$ is the full complex action. In our Born–Fokker–Planck approach the phase J_I is not used to determine the particle’s stochastic motion – only the amplitude, or equivalently the real part J_R , is relevant. This difference underscores the simplifying assumption in our method that particle movement is governed solely by the wave function’s modulus, whereas Nelson’s framework incorporates both amplitude and phase in its dual-process formulation.

Using the relation Eq. (3.7), this drift velocity can be written as:

$$\mathbf{v}(\mathbf{x}) = \frac{\hbar}{m} \nabla \log |\psi(\mathbf{x})|. \quad (3.15)$$

Thus, in this formulation, the drift velocity emerges directly from the logarithm of the wave function’s amplitude.

4 Derivation of the Drift Velocity Field for Central Potentials in Spherical Coordinates

The study of Brownian motion on Riemannian manifolds is a rich field intersecting stochastic processes, differential geometry, and partial differential equations. This framework extends standard Brownian motion from Euclidean spaces to curved manifolds, capturing the manifold’s intrinsic geometry. In this work, Brownian motion will be analyzed within Euclidean spaces using curvilinear coordinate systems, where geometric factors arise from the coordinate choice rather than the space’s intrinsic curvature. Importantly, the mathematical formulations in both approaches are equivalent. Pioneering works by mathematicians such as Itô [23, 24, 18], Jørgenson [25], Ikeda and Watanabe [26], Elworthy [27], Hsu [28, 29], and many others have laid the foundation for applying stochastic analysis to geometric contexts.

In this chapter, we build upon the findings of previous studies to derive the stochastic equation of motion for an electron in the field of a hydrogen nucleus.

Brownian motion on a Riemannian manifold M is profoundly influenced by the manifold’s geometry. In stochastic process theory, the behavior of a stochastic process is characterized by its infinitesimal generator, which describes its limiting behavior over infinitesimally small time intervals. For Brownian motion on M , the infinitesimal generator is given by one half of the Laplace–Beltrami operator Δ_M . Following the work of Itô [18], the generator of Brownian motion is expressed as:

$$\frac{1}{2} g^{ij} \nabla_i \nabla_j = \frac{1}{2} g^{ij} \frac{\partial^2}{\partial x^i \partial x^j} - \frac{1}{2} g^{ij} \Gamma_{ij}^k \frac{\partial}{\partial x^k}. \quad (4.1)$$

In Itô’s original formulation, the diffusion coefficient is implicitly embedded within the metric tensor g^{ij} . To make the diffusion coefficient explicit, we introduce a scalar diffusion coefficient σ and adjust the stochastic differential equation accordingly. We define σ_k^i and m^k by:

$$\sigma^2 \sum_k \sigma_k^i \sigma_k^j = g^{ij}, \quad (4.2)$$

$$\sigma^2 m^k = -\frac{1}{2} g^{ij} \Gamma_{ij}^k, \quad (4.3)$$

and solving a stochastic differential equation:

$$dX^i = -\sigma^2 m^i dt + \sigma \sigma_k^i dW^k, \quad (4.4)$$

we can describe the movement of the Brownian particle in curved coordinates.

If the metric tensor g is diagonal, it can be shown that:

$$dX^i = -\sigma^2 m^i dt + \sigma \sqrt{g^{ii}} dW^i. \quad (4.5)$$

Introducing new notation for the diffusion coefficients and the drift velocity due to geometric curvature:

$$\sigma^i = \sigma \sqrt{g^{ii}}, \quad (4.6)$$

$$\mu^i = -\sigma^2 m^i, \quad (4.7)$$

the stochastic equation of motion becomes:

$$dX^i = \mu^i dt + \sigma^i dW^i. \quad (4.8)$$

This form resembles the Cartesian case but with diffusion coefficients and drift velocity related to the metric tensor.

To account for the particle's own drift velocity v^i in Euclidean space – not resulting from curvature – we add an additional drift term:

$$dX^i = \mu^i dt + \sqrt{g^{ii}} v^i dt + \sigma^i dW^i. \quad (4.9)$$

In Euclidean space with local spherical coordinates (r, θ, ϕ) , the non-zero components of the inverse metric tensor are:

$$g^{rr} = 1, \quad g^{\theta\theta} = \frac{1}{r^2}, \quad g^{\phi\phi} = \frac{1}{r^2 \sin^2 \theta}. \quad (4.10)$$

The diffusion coefficients in spherical coordinates, as given by Eq. (4.6) become:

$$\sigma^r = \sigma \sqrt{g^{rr}} = \sigma, \quad \sigma^\theta = \sigma \sqrt{g^{\theta\theta}} = \frac{\sigma}{r}, \quad \sigma^\phi = \sigma \sqrt{g^{\phi\phi}} = \frac{\sigma}{r \sin \theta}. \quad (4.11)$$

Since the metric tensor in spherical coordinates is diagonal then the non-zero Christoffel Symbols involved are:

$$\Gamma_{\theta\theta}^r = -r, \quad \Gamma_{\phi\phi}^r = -r \sin^2 \theta, \quad \Gamma_{\phi\phi}^\theta = -\sin \theta \cos \theta. \quad (4.12)$$

Substituting the non-zero Christoffel symbols and the components of the inverse metric tensor into the Eq. (4.7) for the drift velocity due to curvature, we obtain:

$$\mu^r = \sigma^2 \frac{1}{r}, \quad \mu^\theta = \sigma^2 \frac{\cot \theta}{2r^2}, \quad \mu^\phi = 0. \quad (4.13)$$

Combining the diffusion and drift terms arising from the geometry of the spherical coordinate system, the stochastic equations governing Brownian motion in spherical coordinates are:

$$\begin{aligned} dr &= \left(\frac{\sigma^2}{r} + v_r \right) dt + \sigma dW^r, \\ d\theta &= \left(\frac{\sigma^2 \cot \theta}{2r^2} + \frac{1}{r} v_\theta \right) dt + \frac{\sigma}{r} dW^\theta, \\ d\phi &= \frac{1}{r \sin \theta} v_\phi + \frac{\sigma}{r \sin \theta} dW^\phi, \end{aligned} \quad (4.14)$$

where v_r , v_θ , and v_ϕ are the components of the particle's drift velocity in spherical coordinates.

5 Wave Function-Based Calculation of Drift Velocity Fields for Electrons in Central Potentials

It is well known [30] that the solution to the stationary Schrödinger equation in spherical coordinates for the electron in a central potential is given by:

$$\psi_{n\ell m}(r, \theta, \phi) = R_{n\ell}(r)Y_{\ell m}(\theta, \phi), \quad (5.1)$$

where $R_{n\ell}(r)$ is the radial wave function and $Y_{\ell m}(\theta, \phi)$ represents the spherical harmonics, which constitute the angular part of the wave function.

The spherical harmonics, $Y_{\ell m}(\theta, \phi)$, depend on the angular momentum quantum numbers ℓ and m and can be expressed as:

$$Y_{\ell m}(\theta, \phi) = \Theta_{\ell m}(\theta)\Phi_m(\phi), \quad (5.2)$$

where $\Theta_{\ell m}(\theta)$ are the normalized associated Legendre polynomials $P_\ell^m(\cos \theta)$ (see Eq. (A.4)), and $\Phi_m(\phi)$ is the azimuthal function (see Eq. (A.5)).

Note that by utilizing real spherical harmonics, the wave function can be expressed as a real-valued function for any quantum numbers n , ℓ , and m . For more details, see Appendix A. This is very useful if we want to simulate the hydrogen atom for $m \neq 0$. While numerical results for such cases are not presented in this work, it is important to emphasize that the simulation has been successfully tested, for instance, for the $(2, 1, 1)$ state. The implementation and further details can be found in the provided source code [31].

In this paper, we will typically use the notation (n, l, m) to represent the quantum state of the electron. For example, the state with $n = 2, l = 1$, and $m = 0$ will be written as $(2, 1, 0)$.

To determine the drift velocity field in stochastic equation of motion, we will utilize Eqs. (3.15), (5.1) and (5.2), we obtain:

$$\mathbf{v} = \frac{\hbar}{m} \nabla \log (R_{n\ell}(r)\Theta_{\ell m}(\theta)\Phi_m(\phi)). \quad (5.3)$$

Applying the gradient operator in spherical coordinates, we derive:

$$\mathbf{v} = \frac{\hbar}{m} \frac{d}{dr} \log R_{n\ell}(r)\hat{r} + \frac{\hbar}{m} \frac{1}{r} \frac{d}{d\theta} \log \Theta_{\ell m}(\theta)\hat{\theta} + \frac{\hbar}{m} \frac{1}{r \sin \theta} \frac{d}{d\phi} \log (\Phi_m(\phi))\hat{\phi}. \quad (5.4)$$

The final expression for the optimal velocity field $\mathbf{v} = (v_r, v_\theta, v_\phi)$ is:

$$\begin{aligned} v_r &= \frac{\hbar}{m} \left(\frac{1}{R_{n\ell}(r)} \frac{dR_{n\ell}(r)}{dr} \right), \\ v_\theta &= \frac{\hbar}{m} \frac{1}{r} \left(\frac{1}{\Theta_{\ell m}(\theta)} \frac{d\Theta_{\ell m}(\theta)}{d\theta} \right), \\ v_\phi &= \frac{\hbar}{m} \frac{1}{r \sin \theta} \left(\frac{1}{\Phi_m(\phi)} \frac{d\Phi_m(\phi)}{d\phi} \right). \end{aligned} \quad (5.5)$$

6 Calculating Average Radial Kinetic Energy Using a Stochastic Approach

In quantum mechanics, the kinetic energy of an electron is determined by applying the kinetic energy operator and computing its expectation value through the corresponding integral (see Eq. B.2). For a detailed derivation of the kinetic energy using the operator approach, refer to Appendix B.

In contrast, Born-Fokker-Planck Stochastic QM we can define the kinetic energy of the electron not as a Hermitian operator but as the classical kinetic energy of a particle:

$$T_r = \frac{1}{2}m_e v_r^2. \quad (6.1)$$

In this section, we show for the first time that the radial kinetic energy calculated using both the operator approach and the stochastic approach yields identical results. In the subsequent sections, we employ numerical simulations to compute the average kinetic energy and show that its value matches those calculated using Eq. B.2 and Eq. 6.2.

The average radial kinetic energy is then calculated by taking the expectation value of T_r with respect to the probability density of the electron's position. This is expressed as:

$$\langle T_r \rangle = \int_0^\infty \int_0^{2\pi} \int_0^\pi [R_{nl}(r)Y_{\ell,m}(\theta, \phi)]^2 T_r r^2 \sin \theta dr d\theta d\phi. \quad (6.2)$$

Separating the angular part, we obtain:

$$\langle T_r \rangle = \frac{1}{2}m_e \int_0^\infty r^2 R_{nl}^2(r) v_r^2 dr \int_0^{2\pi} \int_0^\pi Y_{\ell,m}(\theta, \phi) Y_{\ell,m}(\theta, \phi) \sin \theta d\theta d\phi. \quad (6.3)$$

Using the normalization of spherical harmonics, the angular integral simplifies to unity:

$$\langle T_r \rangle = \frac{\hbar^2}{2m_e} \int_0^\infty r^2 R_{nl}^2(r) \left(\frac{1}{R_{nl}(r)} \frac{dR_{nl}(r)}{dr} \right)^2 dr. \quad (6.4)$$

Therefore, the expression for the average radial kinetic energy reduces to:

$$\langle T_r \rangle = \frac{\hbar^2}{2m_e} \int_0^\infty \left(\frac{d(rR_{nl}(r))}{dr} \right)^2 dr. \quad (6.5)$$

We will now demonstrate that the average radial kinetic energy calculated using the stochastic approach in Eq. (6.5) is equal to that obtained via the operator approach in Eq. (B.4).

Let us introduce the notation:

$$U = rR, \quad U' = R + rR', \quad U'' = 2R' + rR''. \quad (6.6)$$

Next, we perform integration by parts on the following integral:

$$\int_0^\infty U'^2 dr = \int_0^\infty U'U' dr = U'U \Big|_0^\infty - \int_0^\infty UU'' dr. \quad (6.7)$$

Assuming that $R(r)$ vanishes sufficiently rapidly as $r \rightarrow 0$ and $r \rightarrow \infty$, and that its derivatives remain finite, we obtain:

$$U'U \Big|_0^\infty = 0. \quad (6.8)$$

Consequently, the integral simplifies to:

$$\int_0^\infty U'^2 dr = - \int_0^\infty UU'' dr. \quad (6.9)$$

The left-hand side of Eq. (6.9) represents the radial kinetic energy obtained through the stochastic approach:

$$\int U'^2 dr = \int \left(\frac{d(rR)}{dr} \right)^2 dr. \quad (6.10)$$

Conversely, the right-hand side of Eq. (6.9) corresponds to the average kinetic energy obtained via the operator approach:

$$\int UU'' dr = \int rR(2R' + rR'') dr = \int R(2rR' + r^2R'') dr = \int R \frac{d}{dr} \left(r^2 \frac{dR}{dr} \right) dr. \quad (6.11)$$

Finally, we have demonstrated that the average kinetic energy calculated using the stochastic approach in Eq. (6.5) is equal to that obtained via the operator approach in Eq. (B.4):

$$\int \left(\frac{d(rR)}{dr} \right)^2 dr = - \int R \frac{d}{dr} \left(r^2 \frac{dR}{dr} \right) dr. \quad (6.12)$$

7 Calculating Average Angular Kinetic Energy Using a Stochastic Approach

In quantum mechanics, the angular kinetic energy of an electron is determined by applying the angular kinetic energy operator and computing its expectation value through the corresponding integral (see Eq. C.3). For a detailed derivation of the angular kinetic energy using the operator approach, refer to Appendix C.

In contrast, Born-Fokker-Planck Stochastic QM we define the angular kinetic energy of the electron not in terms of a Hermitian operator, but as the classical kinetic energy associated with the particle's angular motion:

$$T_{\text{angular}} = T_\theta + T_\phi, \quad (7.1)$$

where T_θ and T_ϕ are respectively the polar and azimuthal kinetic energies, given by:

$$T_\theta = \frac{1}{2} m_e v_\theta^2, \quad T_\phi = \frac{1}{2} m_e v_\phi^2. \quad (7.2)$$

The average angular kinetic energy is then calculated by taking the expectation value of T_{angular} with respect to the probability density of the electron's position. This is expressed as:

$$\langle T_{\text{angular}} \rangle = \frac{1}{2} m_e \int_0^\infty \int_0^{2\pi} \int_0^\pi [R_{nl}(r) Y_{l,m}(\theta, \phi)]^2 (v_\theta^2 + v_\phi^2) r^2 \sin \theta d\theta d\phi. \quad (7.3)$$

We first compute the polar kinetic energy, which is associated with the motion in the θ direction:

$$\langle T_\theta \rangle = \frac{1}{2} m_e \int_0^\infty [R_{nl}(r)]^2 r^2 dr 2\pi \int_0^\pi \sin(\theta) [\Theta_{\ell m}(\theta)]^2 v_\theta^2 d\theta. \quad (7.4)$$

Using Eq. (5.5), we obtain:

$$\langle T_\theta \rangle = \frac{\hbar^2}{2m_e} \left\langle \frac{1}{r^2} \right\rangle 2\pi \int_0^\pi \sin(\theta) [\Theta_{\ell m}(\theta)]^2 \left(\frac{1}{\Theta_{\ell m}(\theta)} \frac{d\Theta_{\ell m}(\theta)}{d\theta} \right)^2 d\theta. \quad (7.5)$$

It can be proven that:

$$\int_0^\pi \sin(\theta) \left(\frac{dP_\ell^m(\theta)}{d\theta} \right)^2 d\theta = \frac{(l+m)!}{(l-m)!} \frac{2l^2 - 2l(m-1) - m}{2l+1}. \quad (7.6)$$

Using equations (A.4), (7.6), and (7.5), we present, for the first time, a derivation of the electron's average polar kinetic energy in a central potential using a stochastic approach:

$$\langle T_\theta \rangle = \frac{\hbar^2}{2m_e} \left\langle \frac{1}{r^2} \right\rangle \frac{2l^2 - 2l(m-1) - m}{2}. \quad (7.7)$$

Next, we compute the azimuthal kinetic energy, which is associated with the motion in the ϕ direction:

$$\langle T_\phi \rangle = \frac{1}{2} m_e \int_0^\infty [R_{nl}(r)]^2 r^2 dr \int_0^\pi \sin(\theta) [\Theta_{\ell m}(\theta)]^2 d\theta \int_0^{2\pi} [\Phi_m(\phi)]^2 v_\phi^2 d\phi. \quad (7.8)$$

Using Eq. (5.5), we obtain:

$$\langle T_\phi \rangle = \frac{\hbar^2}{2m_e} \left\langle \frac{1}{r^2} \right\rangle \int_0^\pi \frac{1}{\sin(\theta)} [\Theta_{\ell m}(\theta)]^2 d\theta \int_0^{2\pi} [\Phi_m(\phi)]^2 \left(\frac{1}{\Phi_m(\phi)} \frac{d\Phi_m(\phi)}{d\phi} \right)^2 d\phi. \quad (7.9)$$

It can be proven that:

$$\int_0^\pi \frac{1}{\sin(\theta)} [P_\ell^m(\theta)]^2 d\theta = \frac{(l+m)!}{(l-m)!} \frac{1}{m}. \quad (7.10)$$

Using equations (A.4), (7.10), and (7.9), we calculate the azimuthal kinetic energy as:

$$\langle T_\phi \rangle = \frac{\hbar^2}{2m_e} \left\langle \frac{1}{r^2} \right\rangle \frac{2l+1}{4\pi} \frac{1}{m} \int_0^{2\pi} \left(\frac{d\Phi_m(\phi)}{d\phi} \right)^2 d\phi. \quad (7.11)$$

From the definition of the function $\Phi_m(\phi)$ in Eq. (A.5), it can be easily verified that the value of the last integral is $2\pi m^2$. Consequently, the final result for the azimuthal kinetic energy is:

$$\langle T_\phi \rangle = \frac{\hbar^2}{2m_e} \left\langle \frac{1}{r^2} \right\rangle \frac{2l+1}{2} m. \quad (7.12)$$

Using the equation for the polar kinetic energy (7.7) and the equation for the azimuthal kinetic energy (7.12), we calculate the total angular kinetic energy as:

$$\langle T_{\text{angular}} \rangle = \langle T_\theta \rangle + \langle T_\phi \rangle = \frac{l(l+1)\hbar^2}{2m_e} \left\langle \frac{1}{r^2} \right\rangle. \quad (7.13)$$

While the average polar and azimuthal kinetic energies depend on the magnetic quantum number m , this dependence cancels out when summing both energies to determine the total angular kinetic energy. Consequently, the result for the angular kinetic energy obtained using the stochastic approach matches the result obtained via the operator approach in Eq. (C.6).

8 Simulation of the Hydrogen Atom Using Brownian Motion

In the present study, we develop a computer simulation based on the Born-Fokker-Planck Stochastic QM framework to model the hydrogen atom. In the subsequent sections, we present numerical results that conceptualize the electron as a particle undergoing Brownian motion within the hydrogen atom, rather than being described solely by a wave function. Our approach demonstrates that the wave function can be interpreted as a tool for calculating the electron's optimal drift velocity, and we further show that this microscopic approach, after a sufficient amount of time and statistical averaging, reproduces the probability distributions of the particle's various spherical coordinate components as predicted by the wave function and Bohr rule.

The simulation algorithm is straightforward. We begin by initializing the position of a single electron near the hydrogen nucleus. At each time step, the simulation updates the electron's position using the stochastic equation of motion in spherical coordinates (4.14) and the corresponding drift velocity computed from Eq. (5.5). Alternatively, we merge both equations and introduce, for the first time, a combined stochastic equation of motion for the electron in the hydrogen atom:

$$\begin{aligned} dr &= \frac{\hbar}{m_e} \left(\frac{1}{r} + \left(\frac{1}{R_{n\ell}(r)} \frac{dR_{n\ell}(r)}{dr} \right) \right) dt + \sigma dW^r, \\ d\theta &= \frac{1}{r^2} \frac{\hbar}{m_e} \left(\frac{\cot \theta}{2} + \left(\frac{1}{\Theta_{\ell m}(\theta)} \frac{d\Theta_{\ell m}(\theta)}{d\theta} \right) \right) dt + \frac{\sigma}{r} dW^\theta, \\ d\phi &= \frac{1}{r^2 \sin^2 \theta} \frac{\hbar}{m_e} \left(\frac{1}{\Phi_m(\phi)} \frac{d\Phi_m(\phi)}{d\phi} \right) dt + \frac{\sigma}{r \sin \theta} dW^\phi. \end{aligned} \quad (8.1)$$

We visualize the electron's trajectory in three dimensions and collect statistical data on the radial and angular distributions of its position. After a sufficient simulation time, these distributions converge to the probability distributions (10.1) predicted by the radial and angular wave functions (A.2) and (A.3) and Born rule, respectively. Additionally, we calculate the average energies of the electron and compare our numerical results with the analytical solutions detailed in Sections 6 and 7. This comprehensive approach validates our simulation model and enhances our understanding of the electron's stationary behavior within the hydrogen atom.

The source code for the simulation is implemented in MATLAB and is available on GitHub (see Reference [31]).

9 3D Visualization of the Brownian Motion of the Electron in the Hydrogen Atom

To provide intuition for the reader regarding the Brownian motion of the electron within the hydrogen atom, we present an artificial trajectory of the electron in

Figure 1. In this simulation, we set the stochastic term in the radial stochastic equation of motion (4.14) to zero and simulate the $(1, 0, 0)$ state by initializing the electron's radial coordinate to the Bohr radius, $a_0 = 5.29177 \times 10^{-11}$ m.

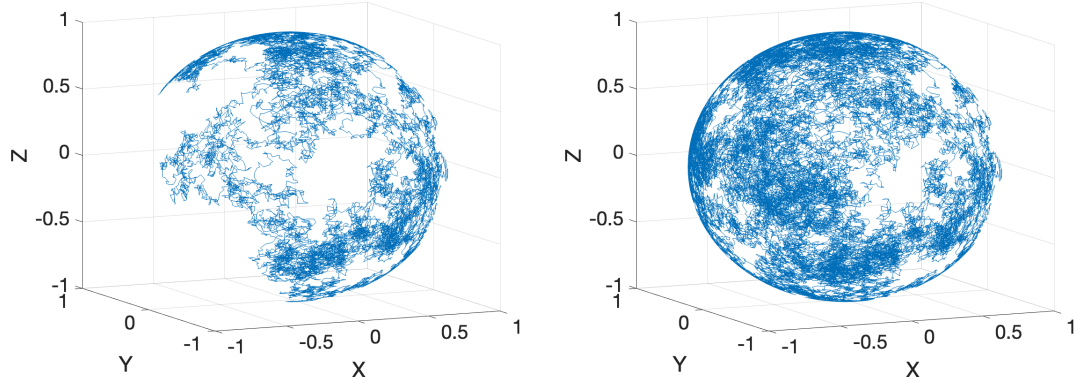


Figure 1: Brownian motion of the electron constrained to a spherical surface. For demonstration purposes, the radial diffusion coefficient is set to zero ($\sigma_r = 0$), resulting in motion confined to a sphere with radius a_0 (Bohr radius). The electron experiences a drift velocity given by $\mathbf{v} = \frac{\hbar}{m_e} \nabla \log \psi_{1,0,0}$. Initially, the electron is positioned on the sphere at spherical coordinates $(a_0, \frac{\pi}{2}, 0)$. **Left:** Electron trajectory at time $t = 2 \times 10^{-16}$ s. **Right:** Electron trajectory at time $t = 5 \times 10^{-16}$ s.

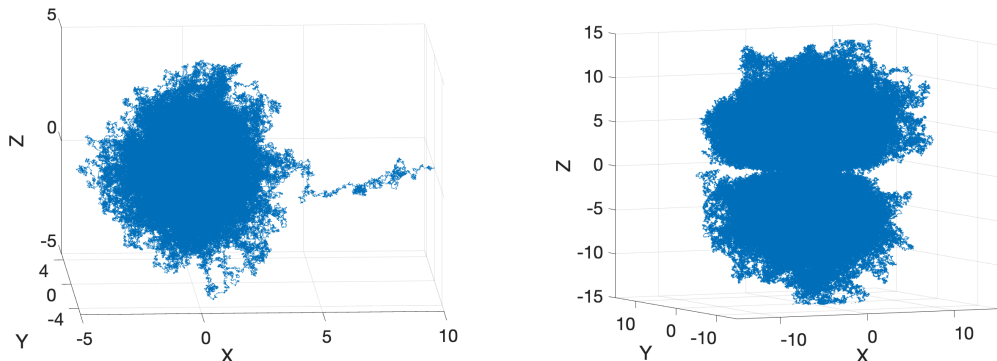


Figure 2: Positions of the electron in three-dimensional space, simulated as a Brownian particle. **Left:** Drift velocity of the electron is: $\mathbf{v} = \frac{\hbar}{m_e} \nabla \log \psi_{1,0,0}$. The electron is initially positioned at the rightmost part of the figure with spherical coordinates $(10 a_0, \frac{\pi}{2}, 0)$ and it drifts toward the nucleus under the influence of Brownian motion. The snapshot represents the electron's position at time $t = 5 \times 10^{-14}$ s. **Right:** Drift velocity field of the electron is: $\mathbf{v} = \frac{\hbar}{m_e} \nabla \log \psi_{2,1,0}$. The figure is at time moment $t = 2 \times 10^{-12}$ s.

This simplification results in an artificial radial movement, enabling the visualization of the electron's Brownian trajectory on a fixed spherical surface. Similar

trajectories of particles constrained to a sphere have been observed in other studies investigating Brownian motion on spherical geometries [32, 33]. However, it is important to note that in reality, Brownian motion encompasses not only movement along a fixed radial distance but also fluctuations in the radial direction.

In the left panel of Figure 2, we position the electron approximately 10 Bohr radii from the center of the hydrogen nucleus and initiate the simulation of the $(1, 0, 0)$ state. The figure demonstrates that the electron drifts toward the nucleus under the influence of Brownian motion. After a few femtoseconds, the electron reaches the Bohr radius and begins to exhibit three-dimensional Brownian motion close around the nucleus.

In the right panel of Figure 2, we present a simulation of the $(2, 1, 0)$ state of the hydrogen atom, generated 2 ps after the simulation commenced. The electron is observed to traverse both lobes of the $(2, 1, 0)$ state. In contrast, shorter simulation durations confine the electron to a single lobe, as evidenced by the polar distribution of the particle's position depicted in Figure 5.

10 Radial, Polar, and Azimuthal Distributions of Electron Positions Around the Atom

If we record the electron's spherical coordinates and create histograms for each coordinate component's distribution, after sufficient time, Figure 3 demonstrates that the radial, polar, and azimuthal distributions of the electron coordinates in the $(1, 0, 0)$ state match the theoretical distributions predicted by Bohr's rule and the theoretical wave function.

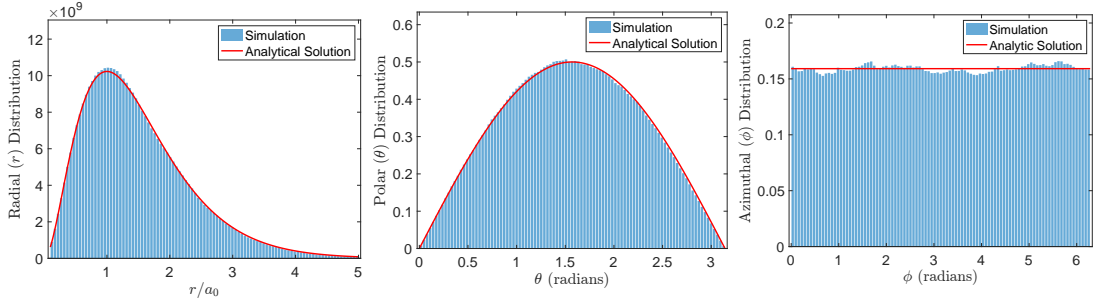


Figure 3: Radial, polar, and azimuthal distributions of the position of the electron, simulated as a Brownian particle moving in the velocity field $\mathbf{v} = \frac{\hbar}{m_e} \nabla \log \psi_{1,0,0}$. The simulation results show good agreement with the analytical result for the normalized probability distribution. The figures are at time moment $t = 5 \times 10^{-13}$ s.

If $R_{n\ell}(r)$ is the radial part of the wave function defined in Eq. (A.2), $\Theta_{\ell m}(\theta)$ is the polar part defined in Eq. (A.4), and $\Phi_m(\phi)$ is the azimuthal part defined in Eq. (A.5), the probability distribution of the electron's spherical components is:

$$\begin{aligned} P_r(r) &= r^2 (R_{n\ell}(r))^2, \\ P_\theta(\theta) &= 2\pi \sin \theta (\Theta_{\ell m}(\theta))^2, \\ P_\phi(\phi) &= \frac{1}{2\pi} (\Phi_m(\phi))^2. \end{aligned} \tag{10.1}$$

In Figure 4, we show the radial and angular distributions of the electron in the $(2, 1, 0)$ state after a sufficiently long simulation time. The simulation results are in good agreement with the theoretical probability densities.

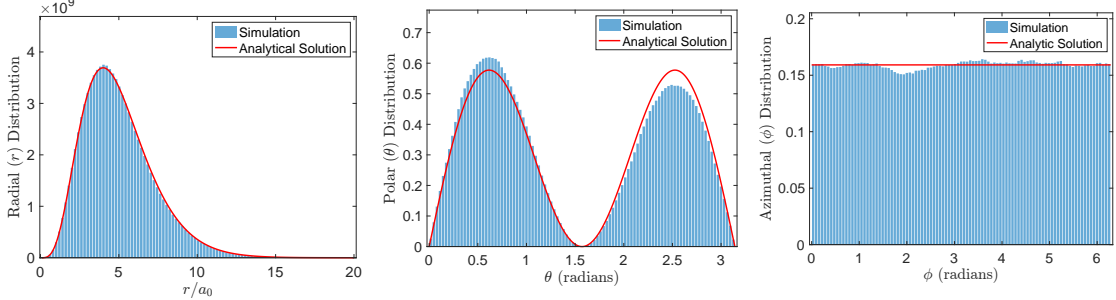


Figure 4: Radial and angular distributions of the position of the electron, simulated as a Brownian particle moving in the velocity field $\mathbf{v} = \frac{\hbar}{m_e} \nabla \log \psi_{2,1,0}$. The simulation results show good agreement with the analytical result for the normalized probability distribution. The figures are at time moment $t = 5 \times 10^{-12}$ s.

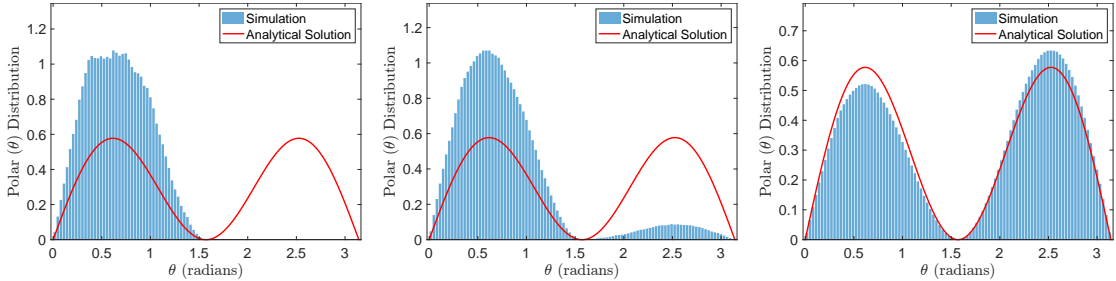


Figure 5: Polar distributions of the electron's position, simulated as a Brownian particle moving in the velocity field $\mathbf{v} = \frac{\hbar}{m_e} \nabla \log \psi_{2,1,0}$. After sufficient time, the simulation results show good agreement with the analytical probability distribution. The figures from left to right correspond to times $t = 1 \times 10^{-13}$ s, $t = 1 \times 10^{-12}$ s, and $t = 1 \times 10^{-11}$ s, respectively.

The polar distribution of the $(2, 1, 0)$ state shown on the right side of Figure 5 follows the theoretical prediction after a sufficiently long simulation time. However, for shorter simulation times, the electron becomes trapped in one of the two lobes, with very rare jumps to the other lobe, as seen in the left side of Figure 5. During the simulation, it is typical to observe an asymmetric polar electron distribution, which becomes symmetric after sufficient simulation time.

The radial distribution of the $(2, 0, 0)$ state shown on the right side of Figure 6 follows the theoretical prediction after a sufficiently long simulation time. Similar to the angular distribution, for shorter simulation times, the electron becomes trapped in one of the two shells, with very rare jumps to the other shell, as seen in the left side of Figure 6.

In Figure 7, we show the deviations of the radial, polar, and azimuthal dis-

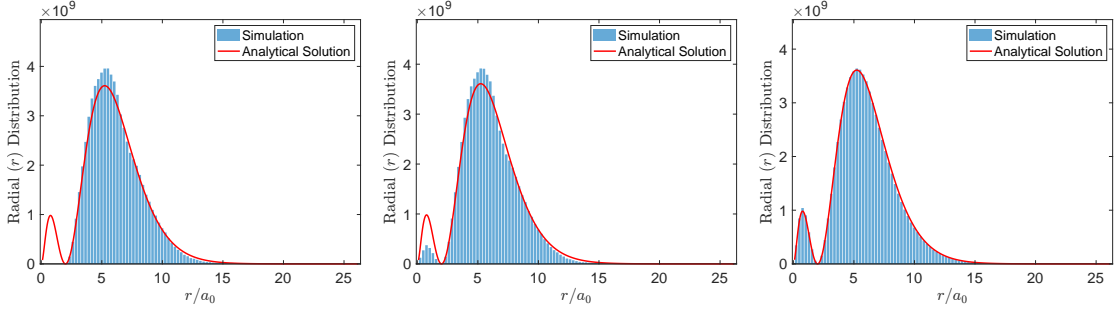


Figure 6: Radial distributions of the electron's position, simulated as a Brownian particle moving in the velocity field $\mathbf{v} = \frac{\hbar}{m_e} \nabla \log \psi_{2,0,0}$. After sufficient time, the simulation results show good agreement with the analytical probability distribution. The figures from left to right correspond to times $t = 3 \times 10^{-13}$ s, $t = 3.2 \times 10^{-13}$ s, and $t = 5 \times 10^{-12}$ s, respectively.

tributions of the electron's positions from the theoretical probability distributions predicted by the wave function and Bohr's rule (see Eq. (10.1)). One can see that for the $(2, 1, 0)$ and $(2, 0, 0)$ states, after a sufficiently long time, the deviations of all distributions become smaller and smaller. This means that we can use the wave function for describing the single electron's position in the hydrogen atom only after sufficient statistical averaging and after times exceeding a few femtoseconds for the radial and azimuthal coordinates distributions and a few picoseconds for the polar coordinates distribution in the case of the $(2, 1, 0)$ state.

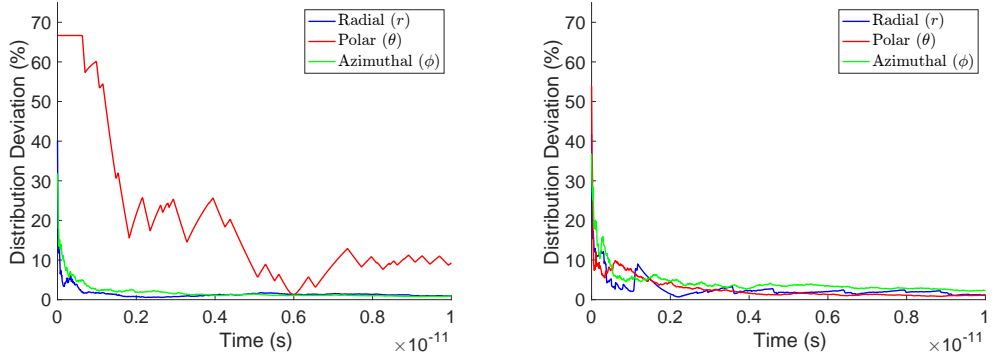


Figure 7: Deviations of the simulated radial and angular distributions from the theoretical distributions predicted by the corresponding wave functions and Born rule. In the left figure, the shown state is the $(2, 1, 0)$ state, and in the right figure, the shown state is the $(2, 0, 0)$ state. After the initial few femtoseconds, the radial and azimuthal distributions, as well as the polar coordinate distributions over a few picoseconds, show only minor deviations from theoretical expectations. The ripples in the polar distribution are attributed to rare transitions of the electron between the two lobes of the $(2, 1, 0)$ state.

11 Kinetic, Potential, and Total Energy of the Electron

By obtaining the velocity and position of the electron at each simulation time step, we can easily compute the radial (T_r), polar (T_θ), and azimuthal (T_ϕ) kinetic energies, as well as the potential energy (V) using simple classical equations of particle energies, as follows:

$$T_r = \frac{1}{2}m_e v_r^2, \quad T_\theta = \frac{1}{2}m_e v_\theta^2, \quad T_\phi = \frac{1}{2}m_e v_\phi^2, \quad V = -\frac{e^2}{4\pi\epsilon_0 r}. \quad (11.1)$$

The total energy is just the sum of all energies:

$$E = T_r + T_\theta + T_\phi + V. \quad (11.2)$$

In this section, we present the results for the average electron energies in the $(2, 1, 0)$ and $(2, 0, 0)$ states of the hydrogen atom. Similar results can be obtained for any other state by running the provided code [31] with different quantum numbers.

The results for the average energies as a function of simulation time are shown in Figure 8.

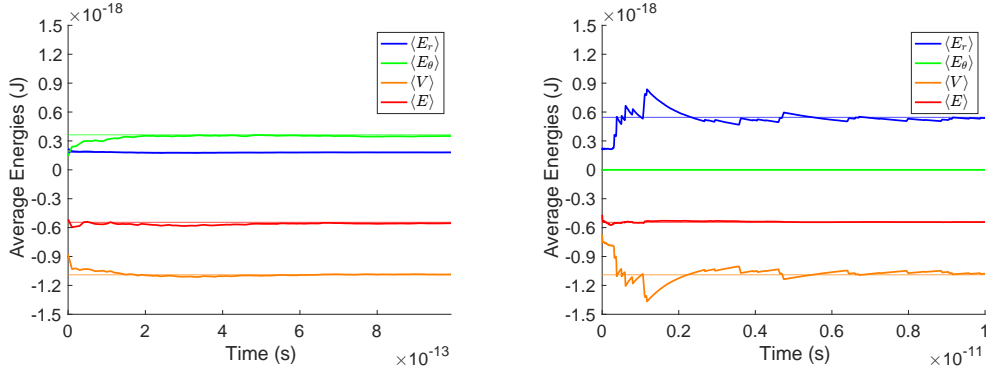


Figure 8: Average radial and angular kinetic energies, along with potential and total energies, of the electron performing Brownian motion with drift velocities defined by $\mathbf{v}_{2,1,0} = \frac{\hbar}{m_e} \nabla \log \psi_{2,1,0}$ and $\mathbf{v}_{2,0,0} = \frac{\hbar}{m_e} \nabla \log \psi_{2,0,0}$, plotted as functions of simulation time for the $(2, 1, 0)$ (left) and $(2, 0, 0)$ (right) states. After a few hundred femtoseconds for $(2, 1, 0)$ state and few picoseconds for $(2, 0, 0)$ state, the simulated energies are observed to converge to their theoretical expectations.

The average radial energy for the chosen atomic state can be calculated easily using the equations (6.5) and the radial wave function (A.2) applied for the state $(2, 1, 0)$ and $(2, 0, 0)$ in our example.

$$\langle T_r \rangle_{2,1,0} = 1.8166 \times 10^{-19} \text{ J}, \quad \langle T_r \rangle_{2,0,0} = 5.4497 \times 10^{-19} \text{ J}. \quad (11.3)$$

In order to calculate the average angular energy, it is necessary first to calculate the average of the reciprocal square of the radial position of the electron for the $(2, 1, 0)$ state:

$$\left\langle \frac{1}{r^2} \right\rangle_{2,1,0} = \int_0^\infty r^2 [R_{21}(r)]^2 \frac{1}{r^2} dr = \frac{1}{12a_0^2} = 2.9759 \times 10^{19} \text{ m}^{-2}. \quad (11.4)$$

The average angular energy for the chosen atomic states can be calculated easily using equations (7.13) and (11.4):

$$\langle T_{\text{angular}} \rangle_{2,1,0} = 3.633 \times 10^{-19} \text{ J}, \quad \langle T_{\text{angular}} \rangle_{2,0,0} = 0 \text{ J}. \quad (11.5)$$

The potential energy of (2, 1, 0) and (2, 0, 0) states be calculated with the following integral:

$$\begin{aligned} \langle V \rangle_{2,1,0} &= -\frac{e^2}{4\pi\epsilon_0} \left\langle \frac{1}{r} \right\rangle_{2,1,0} = -\frac{e^2}{4\pi\epsilon_0} \int_0^\infty r^2 [R_{21}(r)]^2 \frac{1}{r} dr = -\frac{e^2}{4\pi\epsilon_0} \frac{1}{4a_0} = -10.899 \times 10^{-19} \text{ J}, \\ \langle V \rangle_{2,0,0} &= -10.899 \times 10^{-19} \text{ J}. \end{aligned} \quad (11.6)$$

Finally, the total energy of the electron for the (2, 1, 0) and (2, 0, 0) states are:

$$\begin{aligned} \langle E \rangle_{2,1,0} &= \langle T_r \rangle_{2,1,0} + \langle T_{\text{angular}} \rangle_{2,1,0} + \langle V \rangle_{2,1,0} = -5.4494 \times 10^{-19} \text{ J}, \\ \langle E \rangle_{2,0,0} &= -5.4494 \times 10^{-19} \text{ J}. \end{aligned} \quad (11.7)$$

It can be seen from Figure 8 that the calculated values for the average radial and angular kinetic energies, potential energy, and total energy in equations (11.3), (11.5), (11.6), and (11.7) are in good agreement with the corresponding energies of the electron computed from the computer simulation after sufficient time.

12 Analysis of Stability and Convergence in Stochastic Simulations

From Eqs. (5.5) and (8.1), we observe that both the particle's own drift velocity and the drift velocity arising from the curved coordinate system become unbounded as the corresponding wave functions approach zero – $R_{n\ell}(r) = 0$, $\Theta_{\ell m}(\theta) = 0$, and $\Phi_m(\phi) = 0$ – as well as at the coordinates $r = 0$ and $\theta = \frac{\pi}{2}$ due to the curved coordinate system. In this study, we perform stochastic simulations of the (1, 0, 0), (2, 0, 0), and (2, 1, 0) quantum states. The wave functions that vanish within the interior of their domains are $R_{2,0}(r)$ and $\Theta_{1,0}(\theta)$. To ensure numerical convergence and stability of the simulations – particularly concerning the radial kinetic energy associated with the (2, 0, 0) state and the polar kinetic energy associated with the (2, 1, 0) state – additional constraints are necessary. Specifically, imposing restrictions on the particle's radial and polar drift velocities is crucial for achieving convergence in the computed average radial and polar kinetic energy.

This section focuses on the stability and numerical convergence of the stochastic simulations, with particular emphasis on the average polar kinetic energy of the (2, 1, 0) state. The methods and conclusions presented here are also applicable to other electronic states. We derive the probability distributions of the electron's polar kinetic energy and analyze their statistical properties, including the first and second moments.

To determine the polar kinetic energy, we start from Eqs. (5.5) and (A.4), recalling that $P_1^0(\cos \theta) = \cos \theta$. For the (2, 1, 0) state, we find:

$$v_\theta = -\frac{\hbar}{m_e r} \tan \theta. \quad (12.1)$$

From Eqs. (7.2) and (12.1), the polar kinetic energy of the electron in $(2, 1, 0)$ state is:

$$T_\theta = \frac{\hbar^2}{2m_e r^2} \tan^2 \theta. \quad (12.2)$$

Initially, we treat r as a constant to simplify the analysis. Later, we will relax this assumption and consider r as a random variable. Using Eqs. (10.1) and (A.4), the probability distribution of θ in the $(2, 1, 0)$ state is:

$$P_\theta(\theta) = \frac{3}{2} \sin \theta \cos^2 \theta. \quad (12.3)$$

We employ the standard transformation of random variables for probability densities [34] to derive the probability distribution of the polar kinetic energy:

$$P_{T_\theta}(T_\theta) = \sum_{\theta_i: T_\theta(\theta_i)=T_\theta} P_\theta(\theta_i) \left| \frac{d\theta_i}{dT_\theta} \right|, \quad (12.4)$$

where the summation runs over each distinct solution θ_i that satisfies $T_\theta(\theta_i) = T_\theta$. Each solution θ_i corresponds to a separate branch of the inverse function $\theta(T_\theta)$. These branches are defined within the distinct monotonic segments of the original function $T_\theta(\theta)$, ensuring that the inverse remains well-defined and single-valued within each segment.

The branches of the inverse function $\theta(T_\theta)$ are defined as:

$$\theta_1(T_\theta) = \arctan \sqrt{\frac{2m_e r^2}{\hbar^2} T_\theta}, \quad 0 \leq \theta_1 \leq \frac{\pi}{2} \quad (12.5)$$

$$\theta_2(T_\theta) = \pi - \arctan \sqrt{\frac{2m_e r^2}{\hbar^2} T_\theta}, \quad \frac{\pi}{2} \leq \theta_2 \leq \pi \quad (12.6)$$

For both branches, the probability density function $P_\theta(\theta_i)$ is identical and given by:

$$P_\theta(\theta_i) = \frac{3}{2} \frac{\sqrt{\frac{2m_e r^2}{\hbar^2} T_\theta}}{(1 + \frac{2m_e r^2}{\hbar^2} T_\theta)^{3/2}}. \quad (12.7)$$

The absolute value of the derivative with respect to T_θ is the same for both branches:

$$\left| \frac{d\theta_1}{dT_\theta} \right| = \left| \frac{d\theta_2}{dT_\theta} \right| = \frac{2m_e r^2}{\hbar^2} \frac{1}{2\sqrt{\frac{2m_e r^2}{\hbar^2} T_\theta} \left(1 + \frac{2m_e r^2}{\hbar^2} T_\theta\right)}. \quad (12.8)$$

Substituting these expressions into the Eq. (12.4), we obtain the probability distribution of the polar kinetic energy:

$$P(T_\theta) = \frac{3}{2} \frac{2m_e r^2}{\hbar^2} \left[1 + \frac{2m_e r^2}{\hbar^2} T_\theta \right]^{-\frac{5}{2}}. \quad (12.9)$$

This energy distribution is known as the Lomax (Pareto Type II) distribution [35]. It is a heavy-tailed probability distribution with a finite mean but an infinite variance.

Next, consider the case where r itself is a random variable. We now have:

$$P_{T_\theta}(T_\theta) = \int_0^\infty P_{T_\theta}(T_\theta \mid r) P_{r,(2,1)}(r) dr. \quad (12.10)$$

The radial distribution for the $(2, 1, 0)$ state can be obtained from Eqs.(10.1) and (A.2), which appear to be given by the gamma distribution [34]:

$$P_{r,(2,1)}(r) = \frac{r^4}{24a_0^5} e^{-\frac{r}{a_0}}. \quad (12.11)$$

For large T_θ , we have:

$$P(T_\theta) \sim (T_\theta)^{-\frac{5}{2}} \int_0^\infty r^{-3} P_{r,(2,1)}(r) dr. \quad (12.12)$$

The integral $\int_0^\infty r^{-3} P_{r,(2,1)}(r) dr$ is finite and does not depend on T_θ , leaving the asymptotic form of $P(T_\theta)$ unchanged. Thus, even with r as a random variable, the heavy-tailed behavior with exponent $-\frac{5}{2}$ persists, and the variance remains infinite.

To address this convergence issue and ensure stable numerical averages of the polar kinetic energy, we must effectively truncate the heavy tail. One physically motivated approach is to impose a relativistic speed limit on the electron. In the simulation code, we implement the following simple condition:

$$\text{if } |v_\theta| > c \text{ then } v_\theta = c \operatorname{sgn} v_\theta, \quad (12.13)$$

where c is the speed of light, sgn is the sign operator. This constraint “cuts off” the distribution at high velocities, ensuring that the polar kinetic energy does not extend into an unphysical regime. As a result, the previously divergent second moment becomes finite, improving the convergency of the average polar kinetic energy in the simulations.

The lack of convergence of the average polar kinetic energy indicates that, in order to accurately simulate this quantity for the electron, the framework of Born-Fokker-Planck Stochastic QM must incorporate a relativistic treatment of the problem. In future work, we plan to simulate the electron’s Brownian motion within a fully relativistic framework, thereby eliminating the need for such ad hoc constraints.

13 Conclusion

In this work, we have presented an alternative stochastic framework for describing the electron in the hydrogen atom. Rather than relying solely on the conventional probabilistic interpretation and the collapse postulate, our Born-Fokker-Planck Stochastic Quantum Mechanics treats the electron as a Brownian particle with a drift velocity derived directly from the wave function. In our approach, the Born rule serves as the fundamental basis for the probability distribution, and our numerical simulations confirm that the statistical behavior of the electron’s trajectories is consistent with it.

We derived a single real-valued stochastic equation of motion that reproduces the correct average radial and angular kinetic energies, as well as the energy spectrum predicted by standard quantum mechanics. By expressing Brownian motion in

spherical coordinates, we capture the intrinsic geometry of the hydrogen atom and obtain numerical results that converge to the theoretical probability distributions.

Our simulations confirm that, with sufficient ensemble averaging, the stochastic dynamics faithfully reproduce the expected stationary behavior of the electron while physical constraints – such as limiting the drift velocity – ensure numerical stability. This work offers a novel perspective that bridges classical intuitions of particle trajectories with the probabilistic formalism of quantum mechanics.

Future research will extend this approach to non-stationary and relativistic regimes, potentially offering deeper insights into quantum dynamics and guiding the development of advanced experimental techniques such as weak measurements.

A Stationary Wave Function of the Electron in the Hydrogen Atom

The wave function of an electron in a hydrogen atom, which is a solution to the stationary Schrödinger equation, can be separated into radial and angular parts, each depending on specific quantum numbers. This appendix provides detailed expressions for both components.

$$\psi_{n\ell m}(r, \theta, \phi) = R_{n\ell}(r)Y_{\ell m}(\theta, \phi), \quad (\text{A.1})$$

where $R_{n\ell}(r)$ is the radial part and $Y_{\ell m}(\theta, \phi)$ is the angular part of the wave function.

The radial part of the wave function depends on the quantum numbers n (principal quantum number) and ℓ (orbital angular momentum quantum number):

$$R_{n\ell}(r) = \sqrt{\left(\frac{2}{na_0}\right)^3 \frac{(n-\ell-1)!}{2n[(n+\ell)!]^3}} e^{-\frac{r}{na_0}} \left(\frac{2r}{na_0}\right)^\ell L_{n-\ell-1}^{2\ell+1} \left(\frac{2r}{na_0}\right), \quad (\text{A.2})$$

where $a_0 = \frac{4\pi\epsilon_0\hbar^2}{m_e e^2}$ is the Bohr radius, $L_{n-\ell-1}^{2\ell+1}$ are the associated Laguerre polynomials.

The angular part of the wave function is given by the spherical harmonics, which depend on the angular momentum quantum numbers ℓ and m :

$$Y_{\ell m}(\theta, \phi) = \Theta_{\ell m}(\theta)\Phi_m(\phi), \quad (\text{A.3})$$

where the polar part $\Theta_{\ell m}(\theta)$ and the azimuthal function $\Phi_m(\phi)$ are defined as follows:

The polar part is:

$$\Theta_{\ell m}(\theta) = (-1)^m \sqrt{\frac{(2\ell+1)}{4\pi} \frac{(\ell-m)!}{(\ell+m)!}} P_\ell^m(\cos \theta), \quad (\text{A.4})$$

where $P_\ell^m(\cos \theta)$ are the associated Legendre polynomials.

The azimuthal function is [36, 37]:

$$\Phi_m(\phi) = \begin{cases} \sqrt{2} \sin(|m|\phi) & \text{if } m < 0, \\ 1 & \text{if } m = 0, \\ x\sqrt{2} \cos(m\phi) & \text{if } m > 0. \end{cases} \quad (\text{A.5})$$

B Average Radial Kinetic Energy. Operator approach

The operator of the radial kinetic energy is:

$$\hat{T}_r = -\frac{\hbar^2}{2m} \left(\frac{1}{r^2} \frac{d}{dr} \left(r^2 \frac{d}{dr} \right) \right). \quad (\text{B.1})$$

Average Kinetic energy is:

$$\langle T_r \rangle = \int_0^\infty r^2 R_{nl}^*(r) \hat{T}_r R_{nl}(r) dr. \quad (\text{B.2})$$

$$\langle T_r \rangle = \int_0^\infty r^2 R_{nl}^*(r) \left(-\frac{\hbar^2}{2m_e} \frac{1}{r^2} \frac{d}{dr} \left(r^2 \frac{d}{dr} \right) \right) R_{nl}(r) dr. \quad (\text{B.3})$$

Given that $R_{nl}(r)$ is a real function, we can drop the complex conjugate, so we have:

$$\langle T_r \rangle = -\frac{\hbar^2}{2m_e} \int_0^\infty R_{nl}(r) \frac{d}{dr} \left(r^2 \frac{d}{dr} R_{nl}(r) \right) dr. \quad (\text{B.4})$$

C Average Angular Kinetic Energy. Operator approach

The angular kinetic energy is related to the angular part of the Laplacian operator, which, in spherical coordinates, is associated with the angular momentum L^2 . The angular kinetic energy operator can be written as:

$$\hat{T}_{\text{angular}} = \frac{\hat{L}^2}{2m_e r^2}. \quad (\text{C.1})$$

The expectation value of the angular kinetic energy is computed by integrating over the angular part of the wave function and applying the angular kinetic energy operator:

$$\langle T_{\text{angular}} \rangle = \int_0^\infty \int_0^{2\pi} \int_0^\pi R_{nl}(r) Y_{l,m}(\theta, \phi) \hat{T}_{\text{angular}} R_{nl}(r) Y_{l,m}(\theta, \phi) r^2 \sin \theta d\theta d\phi. \quad (\text{C.2})$$

Since $\hat{L}^2 Y_{l,m}(\theta, \phi) = l(l+1)\hbar^2 Y_{l,m}(\theta, \phi)$, we can write:

$$\langle T_{\text{angular}} \rangle = \frac{l(l+1)\hbar^2}{2m_e} \int_0^\infty r^2 R_{nl}^2(r) \frac{1}{r^2} dr \int_0^{2\pi} \int_0^\pi |Y_{l,m}(\theta, \phi)|^2 \sin \theta d\theta d\phi. \quad (\text{C.3})$$

Spherical harmonics are orthogonal over the angular domain:

$$\int_0^{2\pi} \int_0^\pi Y_{l,m}(\theta, \phi) Y_{l',m'}(\theta, \phi) \sin \theta d\theta d\phi = \delta_{ll'} \delta_{mm'}. \quad (\text{C.4})$$

This means:

$$\int_0^{2\pi} \int_0^\pi |Y_{l,m}(\theta, \phi)|^2 \sin \theta d\theta d\phi = 1. \quad (\text{C.5})$$

Given the orthogonality property, the angular kinetic energy becomes:

$$\langle T_{\text{angular}} \rangle = \frac{l(l+1)\hbar^2}{2m_e} \left\langle \frac{1}{r^2} \right\rangle. \quad (\text{C.6})$$

The radial wave function $R_{nl}(r)$ for hydrogen is known to be of the form:

$$R_{nl}(r) = \frac{1}{(2l+1)!} \left(\frac{2r}{na_0} \right)^l L_{n-l-1}^{2l+1} \left(\frac{2r}{na_0} \right) e^{-r/(na_0)}, \quad (\text{C.7})$$

where L_{n-l-1}^{2l+1} are associated Laguerre polynomials.

Acknowledgments

The author expresses sincere gratitude to Prof. Asen Pashov and Asst. Prof. Lachezar Simeonov for their insightful discussions, which made valuable contributions to the improvement of this work.

Bibliography

- [1] J.J. Thomson. Xxiv. on the structure of the atom: an investigation of the stability and periods of oscillation of a number of corpuscles arranged at equal intervals around the circumference of a circle; with application of the results to the theory of atomic structure. *The London, Edinburgh, and Dublin Philosophical Magazine and Journal of Science*, 7(39):237–265, 1904. doi: 10.1080/14786440409463107.
- [2] E. Rutherford. Lxxix. the scattering of α and β particles by matter and the structure of the atom. *The London, Edinburgh, and Dublin Philosophical Magazine and Journal of Science*, 21(125):669–688, 1911. doi: 10.1080/14786440508637080.
- [3] N. Bohr. I. on the constitution of atoms and molecules. *The London, Edinburgh, and Dublin Philosophical Magazine and Journal of Science*, 26(151):1–25, 1913. doi: 10.1080/14786441308634955.
- [4] E. Schrödinger. An undulatory theory of the mechanics of atoms and molecules. *Phys. Rev.*, 28:1049–1070, Dec 1926. doi: 10.1103/PhysRev.28.1049.
- [5] Travis Norsen. *Foundations of Quantum Mechanics: An Exploration of the Physical Meaning of Quantum Theory*. Undergraduate Lecture Notes in Physics. Springer, 1st edition, 2017. ISBN 978-3-319-65866-7. doi: 10.1007/978-3-319-65867-4.
- [6] Yakir Aharonov, David Z. Albert, and Lev Vaidman. How the result of a measurement of a component of the spin of a spin-1/2 particle can turn out to be 100. *Phys. Rev. Lett.*, 60:1351–1354, Apr 1988. doi: 10.1103/PhysRevLett.60.1351.
- [7] H M Wiseman. Grounding bohmian mechanics in weak values and bayesianism. *New Journal of Physics*, 9(6):165, jun 2007. doi: 10.1088/1367-2630/9/6/165.

- [8] Justin Dressel, Mehul Malik, Filippo M. Miatto, Andrew N. Jordan, and Robert W. Boyd. Colloquium: Understanding quantum weak values: Basics and applications. *Rev. Mod. Phys.*, 86:307–316, Mar 2014. doi: 10.1103/RevModPhys.86.307.
- [9] Edward Nelson. Derivation of the schrödinger equation from newtonian mechanics. *Phys. Rev.*, 150:1079–1085, Oct 1966. doi: 10.1103/PhysRev.150.1079.
- [10] Edward Nelson. *Quantum Fluctuations*. Princeton Series in Physics. Princeton University Press, 1985. ISBN 9780691083797.
- [11] Lech Papiez. Stochastic optimal control and quantum mechanics. *Journal of Mathematical Physics*, 23(6):1017–1019, 06 1982. ISSN 0022-2488. doi: 10.1063/1.525488.
- [12] Ciann-Dong Yang and Lieh-Lieh Cheng. Optimal guidance law in quantum mechanics. *Annals of Physics*, 338:167–185, 2013. ISSN 0003-4916. doi: 10.1016/j.aop.2013.08.001.
- [13] Folkert Kuipers. *Stochastic Mechanics: The Unification of Quantum Mechanics with Brownian Motion*. SpringerBriefs in Physics. Springer, 2023. ISBN 978-3-031-31447-6. doi: 10.1007/978-3-031-31448-3.
- [14] Vasil Yordanov. Derivation of dirac equation from the stochastic optimal control principles of quantum mechanics. *Scientific Reports*, 14(1):6507, 2024. ISSN 2045-2322. doi: 10.1038/s41598-024-56582-5.
- [15] Vasil Yordanov. Complex stochastic optimal control foundation of quantum mechanics. *Physica Scripta*, 99(11):115278, oct 2024. doi: 10.1088/1402-4896/ad87ca.
- [16] A. Truman and J. T. Lewis. The stochastic mechanics of the ground-state of the hydrogen atom. In Philippe Albeverio, Sergio A. and Blanchard and Ludwig Streit, editors, *Stochastic Processes — Mathematics and Physics*, pages 168–179, Berlin, Heidelberg, 1986. Springer Berlin Heidelberg. ISBN 978-3-540-39703-8.
- [17] Daniel W. Stroock. On the growth of stochastic integrals. *Zeitschrift für Wahrscheinlichkeitstheorie und Verwandte Gebiete*, 18(4):340–344, December 1971. ISSN 1432-2064. doi: 10.1007/BF00535035.
- [18] Kiyosi Itô. The brownian motion and tensor fields on riemannian manifold. In *Proceedings of the International Congress of Mathematicians (Stockholm)*, pages 536–539, Stockholm, 1962. URL <https://www.mathunion.org/fileadmin/ICM/Proceedings/ICM1962.1/ICM1962.1.ocr.pdf>.
- [19] Gareth C. Price and David Williams. Rolling with ‘slipping’ : I. In Jacques Azéma and Marc Yor, editors, *Séminaire de Probabilités XVII 1981/82*, pages 194–197, Berlin, Heidelberg, 1983. Springer Berlin Heidelberg. ISBN 978-3-540-39614-7.

- [20] M. van den Berg and J. T. Lewis. Brownian motion on a hypersurface. *Bulletin of the London Mathematical Society*, 17(2):144–150, 03 1985. ISSN 0024-6093. doi: 10.1112/blms/17.2.144.
- [21] Michele Pavon. Hamilton’s principle in stochastic mechanics. *Journal of Mathematical Physics*, 36(12):6774–6800, 12 1995. ISSN 0022-2488. doi: 10.1063/1.531187.
- [22] Jussi Lindgren and Jukka Liukkonen. Quantum mechanics can be understood through stochastic optimization on spacetimes. *Scientific Reports*, 9(1), December 2019. doi: 10.1038/s41598-019-56357-3.
- [23] Kiyosi Itô. Stochastic differential equations in a differentiable manifold. *Nagoya Mathematical Journal*, 1:35 – 47, 1950. doi: 10.1017/S0027763000022819.
- [24] Kiyosi Itô. Stochastic Differential Equations in a Differentiable Manifold (2). *Memoirs of the College of Science, University of Kyoto. Series A: Mathematics*, 28(1):81 – 85, 1953. doi: 10.1215/kjm/1250777513.
- [25] Erik Jorgensen. The central limit problem for geodesic random walks. *Zeitschrift für Wahrscheinlichkeitstheorie und Verwandte Gebiete*, 32(1):1–64, 1975. ISSN 1432-2064. doi: 10.1007/BF00533088.
- [26] Nobuyuki Ikeda and Shinzo Watanabe. *Stochastic Differential Equations and Diffusion Processes*. North Holland, 0 edition, 1981. ISBN 978-0444861726. Hardcover.
- [27] K. D. Elworthy. *Stochastic Differential Equations on Manifolds*. London Mathematical Society Lecture Note Series. Cambridge University Press, Cambridge, 1982. ISBN 9780521287678. doi: 10.1017/CBO9781107325609.
- [28] Pei Hsu. Brownian motion and riemannian geometry. In Rick Durrett and Mark A. Pinsky, editors, *Geometry of Random Motion*, volume 73 of *Contemporary Mathematics*, pages 95–104. American Mathematical Society, Providence, RI, 1988. ISBN 978-0-8218-5081-7.
- [29] Psi Hsu. A brief introduction to brownian motion on a riemannian manifold, 2008. URL <https://people.math.harvard.edu/~ctm/home/text/class/harvard/219/21/html/home/sources/hsu.pdf>. Lecture Notes.
- [30] David J. Griffiths and Darrell F. Schroeter. *Introduction to Quantum Mechanics*. Cambridge University Press, 3rd edition, 2018. ISBN 9781107189638. doi: 10.1017/9781316995433.
- [31] Vasil Yordanov. Modeling the hydrogen atom via brownian motion of the electron, 2024. URL <https://github.com/vasil-yordanov/h-atom-brownian-electron>. Release: 1.0.
- [32] Hank Besser. Brownian manifold. <https://github.com/hankbesser/brownian-manifold>, 2023. Accessed: 2024-04-27.

- [33] Jürgen Angst, Ismaël Bailleul, and Camille Tardif. Kinetic Brownian motion on Riemannian manifolds. *Electronic Journal of Probability*, 20(none):1 – 40, 2015. doi: 10.1214/EJP.v20-4054.
- [34] Athanasios Papoulis and S. Pillai. *Probability, Random Variables and Stochastic Processes*. McGraw-Hill Education, 4th edition, 2001. ISBN 978-0073660110. Hardcover, 864 pages.
- [35] Barry C. Arnold. *Pareto Distributions*. Chapman and Hall/CRC, 2nd edition, 2015. doi: 10.1201/b18141.
- [36] William Thomson and Peter Guthrie Tait. *Treatise on Natural Philosophy*. Cambridge Library Collection - Mathematics. Cambridge University Press, 2nd edition, 2009. ISBN 978-1108005364.
- [37] George B. Arfken, Hans J. Weber, and Frank E. Harris. Chapter 15 - legendre functions. In George B. Arfken, Hans J. Weber, and Frank E. Harris, editors, *Mathematical Methods for Physicists (Seventh Edition)*, pages 715–772. Academic Press, Boston, seventh edition edition, 2013. ISBN 978-0-12-384654-9. doi: 10.1016/B978-0-12-384654-9.00015-3.